Very-low-energy electron-diffraction analysis of oxygen on Cu(001)

S. M. Thurgate and Chang Sun
School of Mathematical and Physical Sciences, Murdoch University, Perth, Western Australia
(Received 3 June 1994; revised manuscript received 6 September 1994)

We have developed a method for adding the effect of the surface barrier to the Van Hove–Tong suite of low-energy electron-diffraction programs enabling us to analyze very-low-energy electron-diffraction (LEED) spectra from complex reconstructed systems. The method models the effect of the surface-potential barrier on the intensities and accurately replicates the fine-structure features found at low energies on many surfaces. It is free from many of the simplifying assumptions made by others attempting to model similar systems. We find that the fine-structure peak positions depend on the inelastic scattering in the barrier region as well as the shape of the real part of the potential barrier. This limits the accuracy of measurement of the shape of the barrier, but useful shape information can be derived from these analyses. We have studied the effect of oxygen overlayers on Cu(001) as well as the clean Cu(001) surface. These surfaces are well described by the model for a range of incident-beam directions. On the oxygen-exposed surface, it is necessary to assume that a $c(2\times2)$ structure exists as a precursor to the $(\sqrt{2}\times2\sqrt{2})R45°$ in order to explain all the data. Further, it is found that the surface-potential barrier moves away from the surface with establishment of the precursor $c(2\times2)$ structure, but then moves back towards the surface as the final $(\sqrt{2}\times2\sqrt{2})R45°$ forms with additional exposure to oxygen. This accounts for the changes in work function with exposure to oxygen found on this surface.

INTRODUCTION

The energy regime below 50 eV is often ignored in low-energy electron-diffraction (LEED) intensity analysis due to a number of complicating effects. These include the appearance of a number of fine-structure features that are due to the effect of trapping electrons in image potential induced surface states. In order to fully account for these features it is necessary to include a full description of the scattering from the surface potential barrier. This must describe the spatial variation in the potential and the multiple scattering that can occur between the potential and the substrate. In this paper we present a model that meets these requirements and interfaces to the Van Hove–Tong[1] suite of LEED programs. These accurately model the effect of a one-dimensional barrier on the intensities and differ from the code our group has used in the past[2] in that (i) they can now be used to examine systems that have more than one atom per unit cell, (ii) the analysis now includes a full description of the multiple scattering between substrate and barrier, and (iii) they calculate accurately the scattering in the top layer, taking into account any variation in the potential of this layer compared to the bulk. These programs are also more general than those of Pfnur, Lindroos, and Menzel[3] as they include a full description of the spatial variation of the surface-potential barrier. They also provide a better description of the scattering than that of Dietz, McRae, and Campbell,[4] as they include an accurate description of the substrate scattering and the effect of multiple scattering in the barrier region.

The model and programs were used to study the scattering from clean Cu(001) and the oxygen exposed Cu(001) surface at very low energies (5–16 eV). Our analysis of the clean surface confirms the barrier parameters proposed by for this surface Dietz, McRae and Campbell,[4] though using the form of the barrier proposed by Jones, Jennings, and Jepsen.[5] The analysis of the oxygen exposed surfaces show that the surface potential is strongly affected by the chemisorption of oxygen and that the fine-structure features due to the barrier are modified by the additional beams induced by the surface reconstruction. This effect has allowed us to determine that there is an intermediate $c(2\times2)$ chemisorbed phase preceding the full reconstruction of the surface into a $(\sqrt{2}\times2\sqrt{2})R45°$ phase. Conventional LEED analyses have been unable to detect the contribution from this phase.[6]

There are four main reasons why energies less than 50 eV are usually ignored in LEED spectra. These include difficulty in convergence of the calculated intensities, features due to nonlinearity in the inelastic potential, such as band-to-band transitions, features in the spectra due to surface-potential barrier effects, and the difficulty in simply acquiring data at such low energies. Pfnur, Lindroos, and Menzel.[3] have looked at two of these issues. They modified a number of the central subroutines of the Van Hove–Tong package to overcome the problem of convergence by employing Kambe's method for the layer summations. They also investigated the influence on the I-V curves from band-to-band transitions. They were able to identify features in I-V curves acquired near normal incidence that were due to band-to-band transitions.

Pfnur, Lindroos, and Menzel,[13] made use of a simple step barrier to account for the influence of the surface-potential barrier on the I-V curves. While it is essential to include some form of a barrier, we have shown previously that one can replicate the details of the barrier-induced features with a model that takes the details of the

spatial variation in the potential into account.

We have previously published details of an electron spectrometer designed to measure *I-V* spectra in this range.[7] It provides a means of gathering the data at high resolution and of determining the incidence angles and contact potential difference. It effectively overcomes the experimental difficulties of measuring data at these low energies.

Despite these problems, there are a number of advantages in analyzing data at very low energies. One needs to consider fewer beams and this can save computation time. The coherence zone is larger for low-energy electrons, making very-low-energy electron diffraction (VLEED) useful in studying systems that are not as well ordered. The scattering from light adsorbates is often weak compared to the scattering from heavier atoms in the substrate, making it difficult to get precise information about their position. At very low energies, the scattering from these becomes comparable with the scattering from heavier atoms. The momentum of the beam is changing rapidly with energy at low energies, so the Bragg features are more closely spaced than at higher energies. Our analysis also shows that additional superstructure beams induced by surface reconstruction highly modify the barrier-induced fine structure. In some circumstances, these can give additional information about the surface structure.

In the work that follows, the structural parameters for the reconstructed surfaces area taken from the literature and no attempt was made to optimize them. Many systematic runs (hundreds) were made with different structural and barrier parameters and it was clear that the VLEED code could distinguish between models with different structures. However, one needs to be careful about relying heavily on the fit in the fine-structure region. The barrier model is a one-dimensional model and so takes no account of the angular momentum of the electrons and the effect any corrugation in the potential might have, particularly on the relative intensity of the fine-structure peaks. We found that it was a relatively straightforward matter to account for the position of the peaks, but on highly reconstructed surfaces, it was not easy to account for their relative intensities. It is also true that the position of the peaks can be influenced by the structural parameters as well as the barrier parameters, so one needs good information about the structure if one is to obtain good information about the shape of the barrier. Nonetheless, in fitting the fine-structure features, one learns more about the surface structure and that the best fit occurs when both the barrier shape and the surface structure are correct.

MODEL

We assume that the surface-potential barrier is represented by a one-dimensional barrier, as in the previous models of other authors.[2–4,12] The structure of the LEED package makes such a potential relatively easy to interface. The scattering from the substrate is assumed to be made up from scattering from a semi-infinite stack of layers.[1] Each layer is represented by a matrix, which quantifies how each beam incident on the layer will be transformed into beams leaving the layer. The scattering from the barrier is represented by a set of matrices representing the transmission and reflection of a set of beams by the barrier. These matrices are added to the substrate reflection matrix using the layer-doubling formalism. This accounts for all possible multiple reflections between the substrate and the barrier. In this formalism, the scattered amplitude from the crystal, with the surface barrier in place, can be written as[5]

$$\mathbf{R}_T^{-+}=\mathbf{r}^{-+}+\mathbf{t}^{-}\mathbf{R}^{-+}(1-\mathbf{r}^{+-}\mathbf{R}^{-+})^{-1}\mathbf{t}^{++} . \quad (1)$$

Here the convention used is that the substrate occupies the positive half space $z>0$ and the superscripts refer to the directions of the electrons, with the second superscript indicating the initial direction and the first indicating the final direction. Hence the total reflection matrix is then $\mathbf{R}_T^{-+}$, while $\mathbf{R}^{-+}$ is the substrate reflection matrix without a barrier and $\mathbf{r}^{-+}$, $\mathbf{r}^{+-}$, $\mathbf{t}^{--}$, and $\mathbf{t}^{++}$ are, respectively, the reflection and transmission matrices of the barrier.

We used the one-dimensional form of the barrier suggested by Jones, Jennings, and Jepsen,[5] as this had given useful insight in the cases we had examined with our one-atom code. The shape of the barrier is given by

$$V=\frac{1-\exp[\lambda(z-z_0)]}{4(z-z_0)} \quad \text{for } z<z_0$$

and

$$V=\frac{-V_0}{A\exp[-B(z-z_0)]+1} \quad \text{for } z\geq z_0 , \quad (2)$$

where $A=4V_0/\lambda-1$ and $B=2V_0/A$ in hartree at. u. This potential takes the form of an image potential for large distances from the surface ($z\ll 0$), but joins smoothly to the inner potential within the substrate. The point at which the potential joins the inner potential is determined by the saturation parameter λ. The position of the classical image plane is given by z_0. The code was organized so that the potential in the top layer was calculated from the shape of the barrier. The top-layer scattering matrix was then calculated using this potential. For the clean surface, it was found that the potential in the top layer was around 3.1 eV different from the substrate inner potential. This is different from our previous calculations,[2] where the top-layer potential was taken to be the same as the potential in the substrate. The inelastic potential could also be set independently in the top layer. The Van Hove–Tong LEED code accommodates this change in the complex inner potential of the top layer, as discussed in Ref. 1, by providing for the separate calculation of the scattering matrix of the top layer, which is then matched to the scattering from the bulk. Pfnur, Lindroos, and Menzel also made their calculations with a different top-layer inner potential.

The mechanism whereby such a potential can give rise to a Rydberg-like set of peaks is well understood and has been reviewed in a number of recent publications.[8] Briefly, the peaks arise from a beam that is pre-emergent. If it has sufficient momentum to have emerged from the

substrate, but not enough to emerge from the crystal's surface-potential barrier, some amplitude can be diffracted into the direction of the measured beam as the beam is turned back onto the crystal by the barrier. This process can continue, with additional amplitude coming from each diffraction event, as illustrated in Fig. 1. The modulation in intensity seen in the I-V curve comes from the interference between these beams. As the energy of the beam increases, the perpendicular momentum of the diffracted beam increases, so the beam travels further from the substrate, increasing the phase change. When the beam energy is very near the emergence energy, a small change in energy causes a large change in phase, so the peaks cluster towards the fixed emergence energy. The surface-potential barrier has a $1/z$ dependence at large distances, identical to the $1/r$ dependence of the Coulomb potential. The $1/z$ dependence from the surface simply reflects the fact that at large distances the surface potential must follow the classical image potential form. The similarity between the surface image potential and the Coulomb potential led early workers to identify these features as a Rydberg series, converging at the emergence energy. Closer consideration shows that the electron damping in the surface region was sufficiently strong to limit the number of fringes to a maximum of about 4.[9] Such nicely defined Rydberg series are only observed when the contribution to the scattered amplitude from barrier scattered beams is coming predominantly from one pre-emergent beam. If more than one beam is involved, then the observed fine structure need not form a Rydberg series at all, as we will illustrate.

We calculated the barrier scattering matrices by integrating the complex-potential Schrödinger equation from the position of the topmost layer of atoms to a point some distance from the surface where the influence of the potential has become insignificant. In order to generate all the required reflection and transmission coefficients, it is also necessary to integrate through the barrier in the opposite direction, starting from outside the surface and integrating to just inside the crystal. The appropriate reflection and transmission coefficients can be found from the value of the wave function and its derivative following this integration, using the following well-known expressions:[8]

$$\mathbf{r}=\frac{ik_\perp\psi+\psi'}{ik_\perp\psi-\psi'}\exp(-2ik_\perp z)\ ,$$
$$\mathbf{t}=\frac{2ik_\perp}{ik_\perp\psi-\psi'}\exp(ik_\perp z)\ , \tag{3}$$

where ψ and ψ' represent the wave function at point z and $k_\perp$ is the perpendicular momentum of the electron. The choice of the integration limits depends on which pair of coefficients is being evaluated. If $\mathbf{r}^{+-}$ and $\mathbf{t}^{--}$ are being evaluated, then the integration of the wave function is started at some large distance from the surface and continued into the point z, which in this case is the surface $z=0$. The choice of where the integration started depended on the energy of the electron compared to the potential. For electrons close to the binding energy, the path was relatively long, around 150 a.u. However, if the energy of the electron was small or large compared with the barrier height, then the path was shortened to around 50 a.u. The other pair of reflection and transmission coefficients was found by reversing the direction of integration in (3). We used the Runga-Kutta technique to integrate through the barrier. This provides both ψ and ψ'. The initial wave function was taken to be a plane wave. The inelastic scattering in the barrier region was modeled with an optical potential with an imaginary component that varied with distance from the surface. The exact form of the imaginary component was given by

$$\mathrm{Im}[V(z)]=\frac{\beta V_i}{1+\exp[\alpha(z-\alpha_2)]}\ , \tag{4}$$

where α and α_2 are fitting parameters, β is a constant, and V_i is the inelastic potential of the top layer. Because the potential is one dimensional, the scattering matrices are all diagonal, as beams cannot be scattered into new beams by the potential. The bulk imaginary potential was taken to be a function of energy and we used the form proposed by McRae and Caldwell:[10]

$$V_{\mathrm{imag}}(E)=-0.26(1+E/\phi)^{1.7}\ . \tag{5}$$

These programs interface seamlessly to the Van Hove–Tong package. We have also found them very useful when incorporated with the code modified by Lindroos to optimize their performance at low energies. In order to use the code, one needs to call upon a routine to calculate the reflection and transmission matrices and then a second routine to add the effect of the surface potential barrier to the calculated substrate reflection matrix.

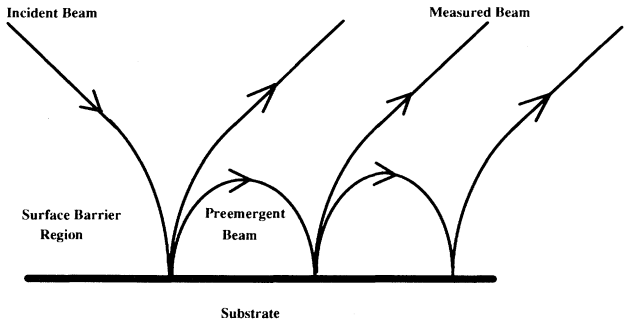

FIG. 1. Mechanism responsible for the production of the fine structure. Part of the amplitude of the incident beam is diffracted into the direction of the measured beam and part into the preemergent beam. The amplitude in the preemergent beam is turned back by the surface potential barrier. Part of this amplitude diffracts back into the direction of the detector, while part diffracts again into the direction of the pre-emergent beam. The measured intensity is the sum of the squares of the amplitude, which ends up at the detector derived from all such events.

ANALYSIS

The data presented here for the Cu(001) surface, both clean and exposed to oxygen, were collected using our

high-resolution VLEED spectrometer.[7] The samples were cut from single crystal Cu and aligned to within 0.5° by Laue backscatter x-ray diffraction. They were polished and electropolished before being introduced to the vacuum chamber. The vacuum chamber had a base pressure of 5×10^{-10} Torr. All samples were cleaned *in situ* by repeated cycles of ion bombardment (Ar ions at 400 eV) and annealing until the surfaces were clean and well ordered as judged by Auger and LEED measurements made with a conventional four grid LEED optics system. All oxygen exposures were made at room temperature without any annealing after the exposure. The exposures were made with an ion gauge switched on, so the exposures should be considered to be to excited oxygen. Further experimental details can be found in Ref. 11.

THE CLEAN Cu(001) SURFACE

There have been several attempts to find the barrier origin and shape parameters for this surface (Hitchen, Thurgate, and Jennings,[2] Dietz, McRae, and Campbell,[4] and Read[12]). There has been some confusion as to how one should include multiple-scattering events between the barrier and the top layer in this system. Dietz, McRae, and Campbell[4] found that they were able to get good fits between experiment and theory if they assumed that there was only one scattering from the barrier. This model become known as the double-diffraction model, as it required two scatterings from the substrate. Their model assumed that the phase change from scattering from the substrate remained constant over the range of energies of the simulation, and they calculated the barrier-induced phase change by integrating the Schrödinger equation in a manner similar to that described above. Hitchen, Thurgate, and Jennings[2] and Read[12] also used the double-diffraction model in their more complete calculations of the scattering from this surface. Read and Christopoulos[13] went on to elaborate the idea more fully in their analysis of the barrier scattering from W(001), concluding that several diffraction events were needed to fully explain the scattering from this surface.

However, it seems that all that is needed is a reasonable description of the surface damping, and the full multiple-scattering formalism gives a good description of the observed features. A comparison between experiment and theory is shown in Fig. 2. The theoretical curves have been convoluted with a Gaussian with a half width of 150 meV, estimated to be our effective resolution under these conditions. The reason why the double-diffraction model gave such good agreement can be seen in Fig. 3. Here the damping in the surface barrier region is increased, with all other parameters remaining constant. As the damping increases, a clear change in the shape of the fine-structure features is seen, particularly around the first peak at 10 eV. This peak shifts to lower energies as the damping increases and higher-order diffraction events make less contribution to the peak shape. We found best agreement between theory and experiment when using large barrier damping values, 2.2 times the bulk damping, for this surface. The reason why such a high value of damping is needed on this surface is not clear. However, the effect is to make the double-diffraction model applicable to this surface, though not necessarily to others, as Dietz, McRae, and Campbell[4] noted. The movement of the first peak with damping is of concern in fitting the fine-structure profile to a model of the surface-potential barrier as it limits the accuracy of any determination of the barrier shape.

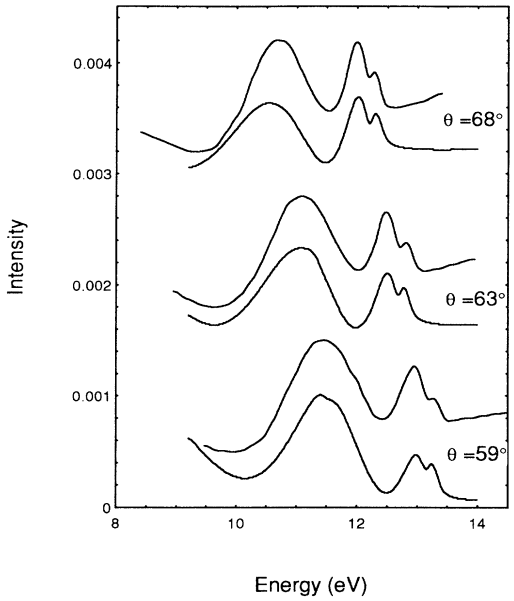

FIG. 2. Comparison between experiment (top curves) and theory (bottom curves) for a range of incident angles with azimuth angle $\varphi=45°$ for the Cu(001) surface. The fitting values are shown in Table I. Intensity is in units of reflectivity.

We used the model of the barrier proposed by Jones, Jennings, and Jepsen[5] as described above. The best-fit values are shown in Table I. The shape of this potential is shown in Fig. 4. As can be seen, the potential in the top layer is some 3.1 eV different from the potential in

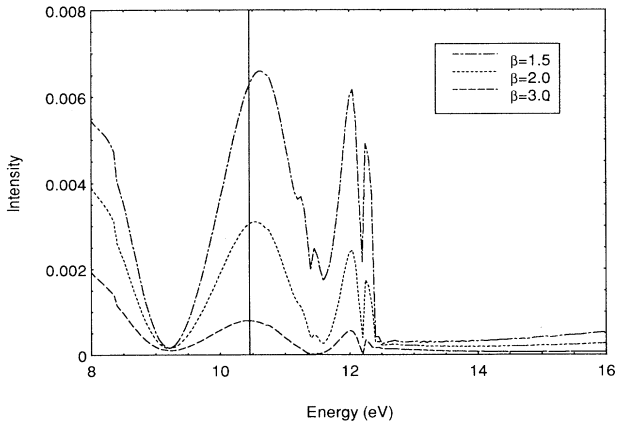

FIG. 3. Effect of surface damping on the fine-structure profile of Cu(001). β is defined by Eq. (4) and is a measure of the strength of the surface barrier damping. Note the effect on peak position. All other parameters are constant.

TABLE I. Best-fit values for the surface barrier parameters for the three surfaces.

	Cu(001)	$c(2\times2)$	$(\sqrt{2}\times2\sqrt{2})R45°$
Z_0 (a.u.)	-3.2 ± 0.2	-4.5 ± 0.2	-4.5 ± 0.2
λ	0.62 ± 0.03	0.68 ± 0.03	0.60 ± 0.03
V (top layer) (eV)	3.10	1.21	2.15

the bulk. This is similar to the result found by Dietz, McRae, and Campbell[4] for this surface, though the estimated that the potential in the top layer was 4.5 eV different from the inner potential. It is interesting to see that this potential has symmetry relative to the jellium edge. The jellium edge is 0.5 lattice spacings in front of the top layer. In the bulk, the charge that comes from the topmost layer can be thought of as occupying this space. In the truncated solid, it can be seen that charge from the top layers has spilled out. As indicated in Fig. 4, the area between the jellium edge, the potential, and the constant inner potential is approximately equal to the area between the potential, the jellium edge, and the vacuum level. This is a consequence of the charge spilling out from the bulk. As the potential is proportional to the square of the charge density, the areas in the figure are equal as far as charge is conserved. It should be recognized, though, that our calculation is insensitive to the shape of the potential for distances into the solid, so the potential in this region is a simple extrapolation of our determinations for $z<0$ given the constraint that it joins the inner potential smoothly at some unknown point inside the crystal.

We were unable to find good agreement with the values for the position of the barrier origin with those found by, Hitchen, Thurgate, and Jennings.[2] The difference between our values and those of Hitchen, Thurgate, and Jennings[2] are explained by the differences in the code of Jones and Jennings,[8] which is the same code used by Hitchen, Thurgate, and Jennings. Jones and Jennings explain in their review paper[8] that they integrate the barrier to a point z_c in the bulk where the potential has become equal to the inner potential. This is in response to the problem that they were unable to use a different inner potential in the top layer. They approximated the effect of the change in potential by integrating the barrier into the solid. However, we are able to calculate the scattering in the top layer with a different inner potential as explained above. Hence we are able to ignore this approximation and integrate only to the topmost layer of atoms.

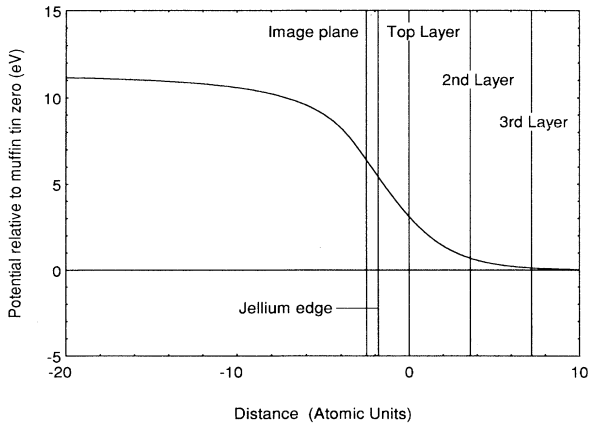

FIG. 4. Surface barrier shape for clean Cu(001). The jellium edge is marked and taken to be half the interlayer spacing in front of the top most layer of atoms. Note the symmetry in the potential about this plane. The position of the image plane is also shown.

OXYGEN ON Cu(001)

Our understanding of the effect of oxygen adsorption on Cu(001) has been uncertain. Early reports suggested that two stable phases were present: a $c(2\times2)$ forming with an exposure of around 300 L and a $(\sqrt{2}\times2\sqrt{2})R45°$ forming around 1000 L. Good agreement has been found in LEED and scanning tunneling microscopy studies of the higher exposure phase and it is now widely accepted that the $(\sqrt{2}\times2\sqrt{2})R45°$ is due to a missing-row system, with the oxygen forming rows of Cu-O. The existence of the $c(2\times2)$ has been questioned in a study by Mayer, Zhoug, and Lynn.[14] They measured the ratio of the intensity of the $\frac{1}{2}$ order to $\frac{1}{4}$ order spots and found that they did not vary with exposure to oxygen. The $\frac{1}{4}$ order spots are found only in the $(\sqrt{2}\times2\sqrt{2})R45°$, while the $\frac{1}{2}$ order spots are common to both structures. Hence they concluded that the $c(2\times2)$ did not exist as a separate phase. This conclusion has been questioned by Lederer *et al.*[15] They used extended x-ray-absorption fine structure to study the absorption of oxygen onto the surface. They found strong evidence that the $c(2\times2)$ did exist, as they measured a nearest-neighbor distance of 1.88 Å, consistent with the $c(2\times2)$ system, with oxygen in the fourfold hollow sites.

We found good agreement between the fine-structure profile on the 1000 L exposed surface and the $(\sqrt{2}\times2\sqrt{2})R45°$ structure. In the calculation, we used the structural parameters from the missing-row model of Zeng and Mitchell.[6] We integrated the surface-potential barrier to the reference plane of atoms, the Cu atoms in this case, in the top layer. Examination of the data shows that exposures intermediate between the clean surface and the 1000 L could not be accounted for by a linear combination of the clean and the $(\sqrt{2}\times2\sqrt{2})R45°$ structure. Hence we attempted to fit the data with a $c(2\times2)$ structure. We used the model proposed by Lederer *et al.*, with oxygen adsorbed into the four-fold hollow sites, 0.8 Å above the surface. We found that a linear combination of the $c(2\times2)$ and the $(\sqrt{2}\times2\sqrt{2})R45°$ structures satisfactorily accounted for all the features observed in experimental results. Comparison between the 250 and 1000 L exposed surface ($\theta=68.5°$ and $\phi=36°$) are shown together with the theoretical spectra for the two structures in Fig. 5. Note that the peak at 8.75 eV is largely absent in the $(\sqrt{2}\times2\sqrt{2})R45°$ structure, but strong in the $c(2\times2)$ structure. It is strong in the 250 L exposed surface, but weak in the 1000 L surface. Similarly, the peak at 11 eV is due to the $c(2\times2)$ structure and is largely absent in the 1000 L exposed surface. This

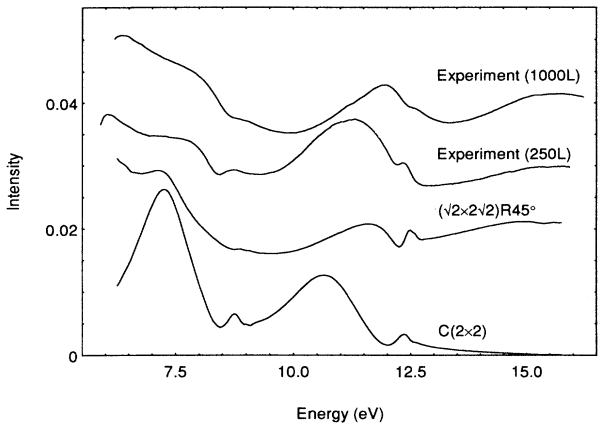

FIG. 5. Effect of oxygen exposure on Cu(001). Experimental *I-V* curves for exposures of 250 and 1000 L of oxygen are shown. Theoretical intensity curves for the Cu(001) $c(2\times2)$ O and the Cu(001) $(\sqrt{2}\times2\sqrt{2})R45°$ O are also shown.

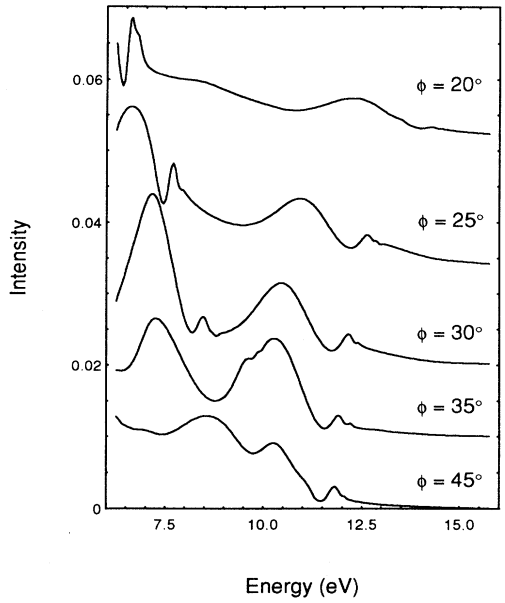

FIG. 7. Effect of changing the azimuthal angle on the calculated intensities of the scattering from the Cu(001) $c(2\times2)$ O surface is shown. The angle of incidence is $\theta=72°$.

effect is also seen in Fig. 6. In these two graphs, the experimental spectra from two different azimuthal angles are shown for a fixed incidence angle of 72° together with the theoretical curves from the two different surface structures. For the symmetric incidence direction of $\phi=45°$, the features from the $c(2\times2)$ are strong, while in the less symmetric direction of $\phi=35°$, the $(\sqrt{2}\times2\sqrt{2})R45°$ features are strong. We were unable to find a unique combination of both structures that gave the correct intensities at all angles for these spectra, though a 50% combination gave the correct position of the peaks.

In Fig. 7 the effect of varying the azimuthal angle on the $c(2\times2)$ surface is shown. The fine structure associated with the $\bar{1}0$ and $0\bar{1}$ emergences can be seen to be dispersing with angle and overlapping near the symmetric position $\phi=45°$. The fine-structure peaks near this symmetric position do not occur in a regular Rydberg series, as they are the result of the superposition of two sets of amplitudes, one due to the $\bar{1}0$ and the other $0\bar{1}$. This produces the features near 12 eV. The best-fit values are shown in Table I.

DISCUSSION

The barrier programs interface well onto the Van Hove–Tong code and explain the observed fine structure and a number of results coming from these analyses. These include the confirmation that the $c(2\times2)$ exists as a precursor to the $(\sqrt{2}\times2\sqrt{2})R45°$. It is clear that the fine-structure profile from the $(\sqrt{2}\times2\sqrt{2})R45°$ does not explain the VLEED spectra observed at intermediate exposures by itself. In order to explain all the features, some admixture of both structures is needed. However, as seen in Fig. 6, it is not a simple linear combination.

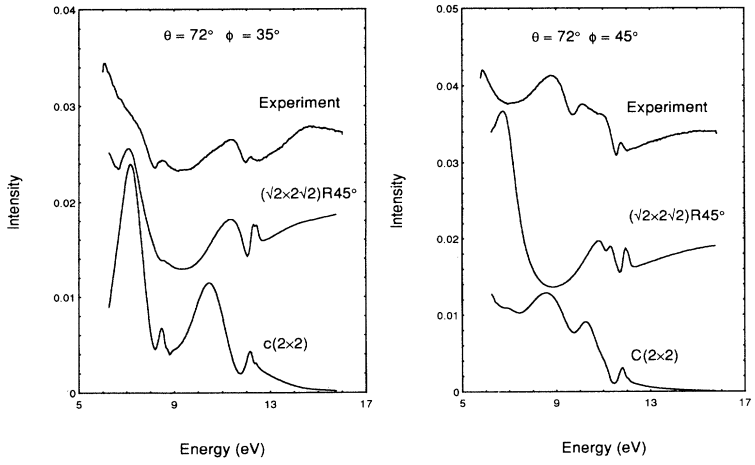

FIG. 6. Comparison of theoretical [Cu(001) $c(2\times2)$ O and Cu(001) $(\sqrt{2}\times2\sqrt{2})R45°$ O structures] and experimental (250 L exposure) *I-V* curves at two different azimuthal angles. Neither theoretical curve fully explains the experimental data, but both curves contain features that are found in the experimental data.

When the incident beam is in the same direction as the missing row of atoms ($\phi=45°$), the scattering from the $(\sqrt{2}\times 2\sqrt{2})R45°$ is suppressed, while at other less symmetric directions, the $(\sqrt{2}\times 2\sqrt{2})R45°$ makes a larger contribution. We suspect that when the beam is incident in these directions, the assumption that the barrier is one dimensional is invalid for the $(\sqrt{2}\times 2\sqrt{2})R45°$, resulting in more intensity being scattered out of the beam.

We propose that the reason why the $c(2\times 2)$ is not seen in conventional LEED is that the surface is somewhat disordered with islands of $c(2\times 2)$ and $(\sqrt{2}\times 2\sqrt{2})R45°$. The spatial coherence width[16] w of an electron beam with a divergence of $\Delta\theta$ and a wavelength of λ is given by

$$w=\frac{\lambda}{\Delta\theta}\ . \tag{6}$$

Hence in the VLEED region where the wavelength of the electrons is comparatively long, the diffraction is from a larger area than conventional LEED and so is more likely to include areas of the surface that have the same structure.

The changes in the shape of the surface barrier that follow oxidation are also of interest. The barrier shapes for the clean and two oxygen exposed surfaces are shown in Fig. 8. As previously noted, the potential on the clean surface is "symmetric" about the jellium edge. The transfer of charge from within the bulk to outside is responsible for the development of the surface dipole layer. As can be seen in Fig. 8, the potential on the oxygen exposed surface is no longer symmetric about the jellium edge. This presumably comes about from the changed electron density in the topmost layer, providing an increased number of electrons to flow out. The change in going from the $c(2\times 2\sqrt{2})R45°$ reflects the change in the atomic density as well as the incorporation of further oxygen in the top layer. The variation in the potential distribution is responsible for the changes in the work function measured on adsorption of oxygen on this face. The fact that the charge moves back towards the surface as the $(\sqrt{2}\times 2\sqrt{2})R45°$ forms is responsible for the reduction in the work function with increasing exposure to oxygen.[17]

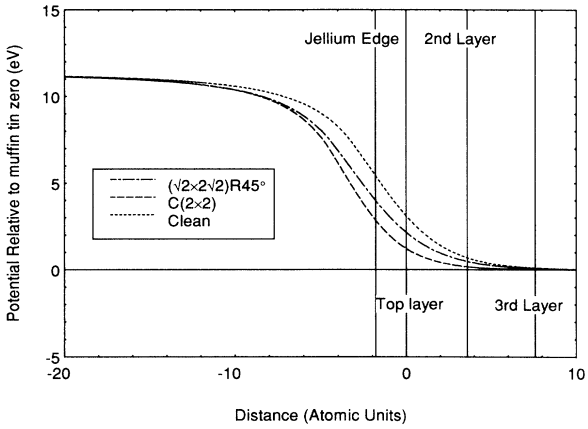

FIG. 8. Comparison of surface-potential barriers for clean Cu(001), Cu(001) $c(2\times 2)$ O, and Cu(001) $(\sqrt{2}\times 2\sqrt{2})R45°$O.

CONCLUSIONS

The calculations reported here are the most complete of their type to date, free from many approximations inherent in previous models. They measure the movement of the surface-potential barrier with oxidation. Beyond that, they show that analysis of VLEED data can be made with a detailed description of the surface-potential barrier for complex, reconstructed surfaces. If the change in the surface geometry creates additional beams that can mix in the barrier region, then the fine structure may give further clues than can be gleaned from analysis of the regular LEED data. The large coherence zone means that VLEED samples the surface on a different size scale than conventional LEED, which may give complementary information. The analysis of VLEED spectra may well have a role to play in the determination of surface structures involving light adsorbates on metals where the scattering from the adsorbate is often weak compared with the scattering from the substrate, as in the case of oxygen on copper. At very low energies, the scattering from light adsorbates is often as strong as the scattering from the substrate atoms.

ACKNOWLEDGMENTS

This project was partly funded by the Australian Research Council and supported by the A. J. Parker cooperative research center in hydrometallurgy. Useful discussions with Phil Jennings contributed much to this work. Our thanks to Matti Lindroos for allowing us to use his computer codes, which formed the basis of much of what we have done here, and to Andris Stelbovics for his critical reading of the manuscript.

[1]M. Van Hove and S. Y. Tong, *Surface Crystallography by LEED* (Springer, Berlin, 1976).
[2]G. J. Hitchen, S. M. Thurgate, and P. J. Jennings, Phys. Rev. B **44**, 3939 (1991).
[3]H. Pfnur, M. Lindroos, and D. Menzel, Surf. Sci. **248**, 1 (1991).
[4]R. E. Deitz, E. G. McRae, and R. L. Campbell, Phys. Rev. Lett. **45**, 1280 (1980).
[5]R. O. Jones, P. J. Jennings, and O. Jepsen, Phys. Rev. B **29**, 6474 (1984).
[6]H. C. Zeng and K. A. R. Mitchell, Surf. Sci. Lett. **239**, L571 (1990).
[7]G. Hitchen and S. M. Thurgate, Phys. Rev. B **38**, 8668 (1988).
[8]R. O. Jones and P. J. Jennings, Surf. Sci. Rep. **9**, 165 (1988).
[9]P. de Andres, P. M. Echenique, and F. Flores, Phys. Rev. B **35**, 4529 (1987).
[10]E. G. McRae and C. W. Caldwell, Surf. Sci. **57**, 766 (1976).

[11]G. Hitchen, S. M. Thurgate, and P. J. Jennings, Aust. J. Phys. **43**, 519 (1990).
[12]M. N. Read, Phys. Rev. B **32**, 2677 (1985).
[13]M. N. Read and A. S. Christopoulos, Phys. Rev. B **37**, 10 407 (1988).
[14]R. Mayer, C. S. Zhoug, and K. G. Lynn, Phys. Rev. B **33**, 8899 (1986).
[15]T. Lederer, D. Arvanitis, G. Comelli, L. Toroger, and K. Baberschke, Phys. Rev. B **48**, 15 390 (1993).
[16]K. Heinz, in *Determination of Surface Structure by LEED,* edited by P. M. Marcus and F. Jona (Plenum, New York, 1984), p. 519.
[17]S. M. Thurgate and P. J. Jennings, Surf. Sci. **131**, 309 (1983).